

# Molecular semiconductor blends: Microstructure, charge carrier transport, and application in photovoltaic cells

Andreas Opitz<sup>\*1</sup>, Julia Wagner<sup>1</sup>, Wolfgang Brütting<sup>1</sup>, Alexander Hinderhofer<sup>2</sup>, and Frank Schreiber<sup>2</sup>

<sup>1</sup>Institute of Physics, University of Augsburg, 86135 Augsburg, Germany

<sup>2</sup>Institute of Applied Physics, University of Tübingen, 72076 Tübingen, Germany

Received 11 May 2009, revised 24 September 2009, accepted 25 September 2009

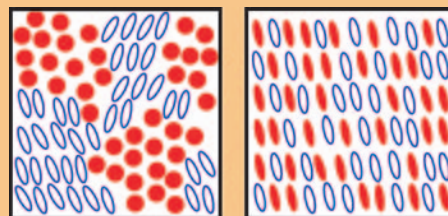
Published online 17 November 2009

PACS 68.55.am, 73.61.Ph, 78.66.Qn, 78.66.Sq, 84.60.Jt

\* Corresponding author: e-mail [Andreas.Opitz@physik.uni-augsburg.de](mailto:Andreas.Opitz@physik.uni-augsburg.de), Phone: +49 821 598 3441, Fax: +49 821 598 3425

Ambipolar organic semiconductor blends, i.e. mixtures of electron and hole conducting materials, attain growing interest due to their utilization in quasi-complementary organic field-effect transistors and organic photovoltaic cells. Many investigations in the latter field have reported an increase of the solar cell efficiency by optimizing the balance between charge carrier transport in phase-separated structures and exciton dissociation at the interface between these phases. Here we show the implications of blending molecular materials for structural, optical, and electrical properties in two model systems for organic photovoltaic cells. We have investigated blends and neat films of the hole transporting material Cu-phthalocyanine (CuPc) together with fullerene C<sub>60</sub> and Cu-hexadecafluorophthalocyanine (F<sub>16</sub>CuPc) as electron transporting materials, respectively. On the one hand, the difference in molecular structure of the spherical C<sub>60</sub> and the planar molecule CuPc leads to nanophase separation in a blend of both of them, causing charge carrier transport being limited by the successful formation of percolation paths. On the other hand, blends of the similar shaped CuPc and F<sub>16</sub>CuPc molecules entail mixed crystalline films, as can be clearly seen by X-ray scattering

measurements. We discuss differences of both systems with respect to their microstructure as well as their electrical transport properties in diodes and field-effect transistors. Furthermore, we compare the photovoltaic properties of planar- and bulk-heterojunction devices under white light illumination to relate the different morphologies of both material systems to their performance in solar cells.



Sketches of different molecular arrangements in blended systems. The formation of phase-separated (left) or molecularly mixed crystalline films (right) can occur, depending on the geometry of the involved molecules.

© 2009 WILEY-VCH Verlag GmbH & Co. KGaA, Weinheim

**1 Introduction** Molecular blends, this means the intentional or unintentional mixture of two organic molecular species are present in a wide range of organic electronic devices [1, 2]. These are, e.g. guest–host systems with low concentration of unintentional impurities or intentionally added dyes or dopants where the matrix carries the current and the dopants are used to modify the emission color or the electrical conductivity. The semiconductor blends discussed here, however, are in a concentration range where both components are active in the charge carrier transport, i.e. above the percolation threshold.

A well-ordered type of molecular blends are charge-transfer crystals, such as TTF-TCNQ and its many derivatives [3]. Due to the low ionization potential of one partner and the high electron affinity of the other one, a (partial) charge transfer from the donor to the acceptor molecule occurs. This ground state charge transfer leads to the dependence of the crystal structure to directions with insulating or conducting properties. When transport takes place, parallel to stacks, with separated donor and acceptor molecules, it will be metallic-like along the stacking direction. It has also been demonstrated that charge transfer

salts can be deposited as crystalline films by thermal evaporation of the bulk material [4].

Another class of blends are thin film mixtures of hole and electron conducting molecules without any charge transfer in the ground state but exhibiting a photoinduced charge transfer when one partner is electronically excited by light absorption. It has been demonstrated that this process occurs on a sub-picosecond time scale in the case of fullerenes as acceptor material [5]. This photo-induced charge transfer is the basis of polymeric or molecular photovoltaic cells where the following four basic steps occur (see Fig. 1) [6]:

- (i) Light absorption/exciton generation ( $\eta_{\text{Abs}}$ ).
- (ii) Exciton diffusion ( $\eta_{\text{ED}}$ ).
- (iii) Charge transfer/exciton dissociation ( $\eta_{\text{CT}}$ ).
- (iv) Charge collection ( $\eta_{\text{CC}}$ ).

Due to the high exciton binding energy in organic systems, the excitons need to dissociate at a donor–acceptor (DA) interface in contrast to inorganic solar cells. The total solar cell efficiency can then be calculated from the product of the efficiencies of the four consecutive steps:

$$\eta = \eta_{\text{Abs}}\eta_{\text{ED}}\eta_{\text{CT}}\eta_{\text{CC}} \quad (1)$$

Organic photovoltaic cells have been used as planar heterojunctions (PHJs) [7] with two successively deposited films or as bulk-heterojunctions (BHJs) [8] with a blended film. Due to limited exciton diffusion length in organic materials, DA blends usually reach higher photocurrents [9, 10]. In PHJ solar cells, excitons need to be closer to the DA interface than the exciton diffusion length in order to dissociate, while in a BHJ, virtually all excitons fulfill this

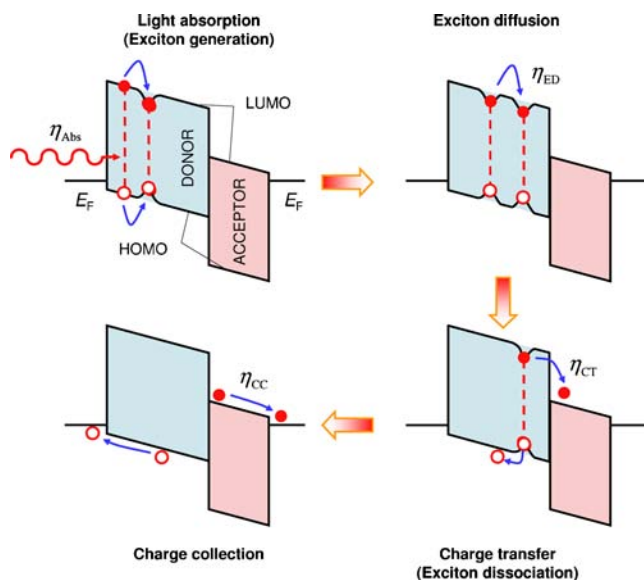


**Figure 1** (online color at: [www.pss-a.com](http://www.pss-a.com)) Basic processes in organic solar cells related to the energy diagram of a DA cell. The  $\eta$ 's give the efficiencies of the individual processes.

condition. So the active volume of the latter type of cells is significantly raised in comparison to PHJ cells of the same material combination.

A number of DA pairs have been implemented in molecular blends for BHJ solar cells. Fullerene  $C_{60}$  has been used as acceptor with different donor materials such as phthalocyanines [11, 12], pentacene [13, 14], or oligothiophenes [15]. Also some perylene derivatives were used as acceptor for solar cells [9]. Complementary optical absorption is advantageous as well as a good transport property of both materials.

Another application of molecular blends of hole and electron conducting molecules are ambipolar organic field-effect transistors (OFETs). Mixtures of phthalocyanine and fullerene were analyzed in ambipolar OFETs and the usability in ambipolar inverters was demonstrated [16]. Furthermore, blends of two electroluminescent materials (oligothiophene and a perylene derivative) have been used as light-emitting OFETs [17]. In both cases, balanced hole and electron mobilities were achieved for certain concentration ratios, giving the best performance of inverters or light-emitting OFETs. Ambipolar transport was also found in neat materials [18–20]; however, there the mobilities cannot be tuned. So mixing of electron and hole transporting materials has the advantage to adjust balanced mobilities by the concentration ratio which is impossible for neat materials.

In this study we present an analysis of two model systems for DA blends. These are (i) copper-phthalocyanine (CuPc) combined with the fullerene  $C_{60}$  and (ii) CuPc in combination with its perfluorinated version ( $F_{16}\text{CuPc}$ ). Thereby CuPc is the donor or *p*-conductor, while  $C_{60}$  and  $F_{16}\text{CuPc}$  are the acceptor materials, which are *n*-conducting. The study comprises structural, optical, and electrical properties of the blends in comparison to the properties of the neat films. Both systems will be examined in solar cells as PHJs and BHJs.

## 2 Materials, devices, and experimental methods

The materials used in this study are copper phthalocyanine (CuPc), purchased from Sigma–Aldrich as sublimation grade and additionally purified by temperature gradient sublimation, as electron donor in combination with Buckminster fullerene ( $C_{60}$ ), purchased from Sigma–Aldrich as sublimation grade, as electron acceptor, as well as perfluorinated CuPc ( $F_{16}\text{CuPc}$ ), purchased from Sigma–Aldrich and additionally purified twice by temperature gradient sublimation, acting also as electron acceptor. The structural formulas are given in Fig. 2a; it is noteworthy that both phthalocyanines are flat molecules, whereas  $C_{60}$  is spherical. The organic semiconductor films were grown by thermal evaporation from low-temperature effusion cells in a vacuum better than  $10^{-7}$  hPa. The film thickness was controlled by using a quartz crystal microbalance. For mixed films, two independent monitors were used. The deposition rates were  $0.35 \text{ \AA/s}$  for neat films and up to  $1.4 \text{ \AA/s}$  for the material with the higher volume fraction in the mixtures.

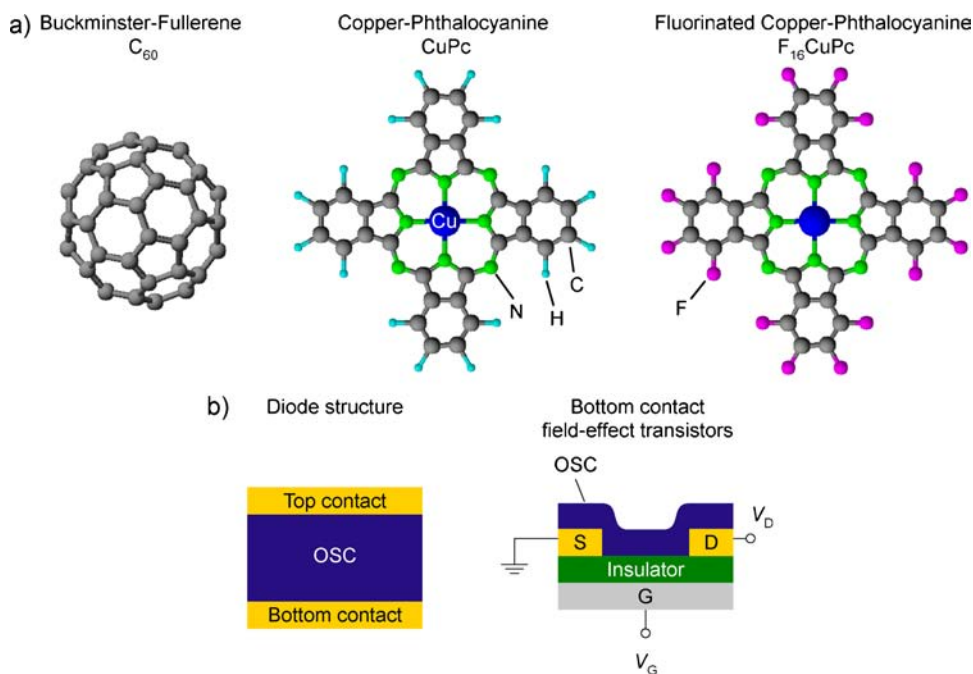


**Figure 2** (online color at: [www.pss-a.com](http://www.pss-a.com)) (a) Molecular materials used in this study: Buckminster fullerene  $C_{60}$ , copper phthalocyanine CuPc, and fluorinated copper phthalocyanine  $F_{16}CuPc$ . (b) Devices used for electrical analysis: diode structure and top-contact bottom-gate field effect-transistor. The organic semiconductor (OSC) can be a neat or a blended layer.

Charge transport properties were analyzed in both unipolar and ambipolar diodes as well as OFETs. All electrical measurements together with the sample transfer were performed under inert conditions or in vacuum. For hole-only diodes, a bottom contact of indium-tin oxide (ITO) covered with 30 nm of the conducting polymer polyethylenedioxythiophene-polystyrenesulfonate (PEDOT:PSS, purchased from H.C. Starck as BAYTRON P, see Fig. 3) was used. The active organic layer was deposited on PEDOT:PSS and thereafter a 40 nm thick *N,N'*-bis(3-methylphenyl)-(1,1'-biphenyl)-4,4'-diamine (TPD, see Fig. 3) film to prevent electron injection from the 30 nm thick gold top electrode. TPD is known as hole-transporting and electron-

blocking layer and can be neglected for the mobility analysis due to its high hole mobility [21]. Alternatively a thin film (1–2 nm) of 2,3,5,6-tetrafluoro-7,7,8,8-tetracyano-quinodimethane ( $F_4TCNQ$ , see Fig. 3) was used. As seen in measurements of field-effect transistors, the  $F_4TCNQ$  layer improves the hole injection [22] and therefore an  $F_4TCNQ/Au$  contact is non-injecting for electrons [20]. The electron-only diodes contain a 30 nm thick Al electrode at the bottom and a 30 nm thick Al electrode on top of the organic film with a 0.5 nm thick interface doping layer of LiF. Using ITO/PEDOT:PSS together with LiF/Al electrodes, ambipolar injection and charge transport occurs. The electrode combinations are summarized in Table 1 together with the resulting transport behavior. The organic semiconductor layer was either a 200 nm (for CuPc/ $C_{60}$ ) or an 80 nm (for CuPc/ $F_{16}CuPc$ ) thick film of neat or blended materials with different mixing ratios and had an active area of about  $2 \times 2 \text{ mm}^2$ .

To analyze the current–voltage characteristics, the measured curves were fitted by the model of trap-free space charge limited current [23] combined with a Poole-Frenkel type field-dependent mobility [24], which gives the current density as

$$j_{SCLC} = \frac{9}{8} \mu_0 \epsilon_0 \epsilon_{osc} \frac{V_{eff}^2}{d^3} \exp \left[ 0.89 \gamma \sqrt{\frac{V_{eff}}{d}} \right]. \quad (2)$$

This dependence contains the zero-field mobility  $\mu_0$  and the field activation parameter  $\gamma$ .  $V_{eff}$  is the effective applied voltage  $V - V_{Bi}$ , with  $V_{Bi}$  being the built-in voltage. The

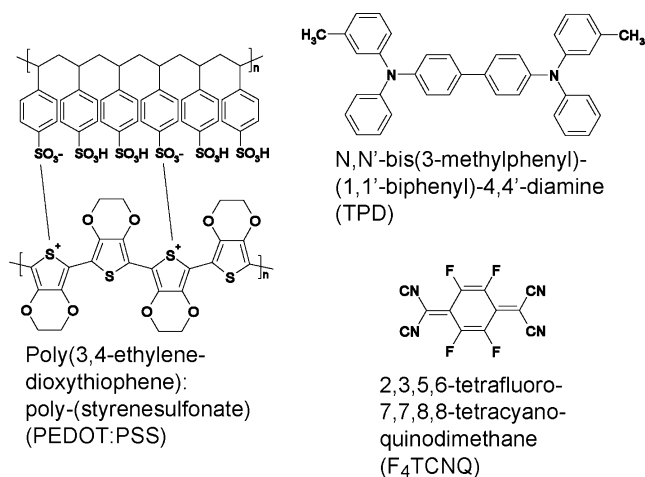


**Figure 3** Structural formula of PEDOT:PSS, TPD, and  $F_4TCNQ$ .

**Table 1** Electrode materials to realize the different transport behaviors in diodes (see Fig. 2b).

transport behavior	bottom electrode	top electrode
unipolar (hole only)	ITO/PEDOT:PSS	F <sub>4</sub> TCNQ/Au or TPD/Au
unipolar (electron only)	Al	LiF/Al
ambipolar	ITO/PEDOT:PSS	LiF/Al

parameters  $\mu_0$ ,  $\gamma$ , and  $V_{Bi}$  are determined by fitting the measurements in the voltage range above about 0.5 V.

OFETs incorporate photolithographically patterned Au (100 nm, using 1 nm Ti as adhesion layer) source and drain electrodes made by electron-beam evaporation and a subsequent lift-off process, as described in Refs. [16, 25]. The channel lengths ranged from 5 to 80  $\mu\text{m}$  with a channel width of 2500  $\mu\text{m}$ . Finally, a 25 nm thick film of the organic materials was deposited on top of these prestructured substrates as described above, to realize a bottom-gate, bottom-contact OFET.

The charge-carrier mobilities  $\mu$  and the threshold voltages  $V_T$  were extracted from the slope of the transfer characteristics in the saturation region  $|V_D| > |V_G - V_T|$  using the standard relationship:

$$I_{D,sat} = \frac{W}{2L} \mu C_{Ox} (V_G - V_T)^2. \quad (3)$$

Here  $W$  is the channel width,  $L$  the channel length,  $C_{Ox}$  the gate-oxide capacitance per unit area,  $V_G$  the gate voltage, and additionally  $V_D$  the drain voltage. Mobility  $\mu$  and threshold voltage  $V_T$  were determined from the linear regression of the measured data plotted as  $\sqrt{I_{D,sat}}$  vs.  $V_G$ .

Additionally, ambipolar diodes with ITO/PEDOT:PSS and LiF/Al as electrodes were investigated as photovoltaic

cells. They had a total organic film thickness of 80 nm, comprising either a 40 nm layer of the acceptor (C<sub>60</sub> or F<sub>16</sub>CuPc) on top of a 40 nm thick CuPc film (“planar heterojunction”) or a 1:1 mixture of both materials (“bulk-heterojunction”). Current–voltage characteristics of the solar cells were measured in darkness and under illumination. The intensity of the solar simulator (AM1.5 filters) ranged up to 100 mW/cm<sup>2</sup>, i.e. one sun.

In addition to the electrical measurements, the neat and blended organic films were analyzed by scanning force microscopy (SFM) and specular X-ray reflectometry. The SFM measurements were performed using a Thermo Microscopes Autoprobe CP-Research in non-contact mode. The X-ray scattering measurements were conducted on a GE/Seifert X-ray diffractometer (Cu  $K\alpha_1$  radiation, multi-layer mirror, and double bounce compressor monochromator). Optical absorption spectra were recorded for films deposited on quartz glass substrates using a Varian UV–Vis spectrophotometer Cary 50. X-ray scattering, SFM, and optical absorption measurements were performed under ambient conditions.

### 3 Experimental results and discussion

**3.1 Structural properties** The film morphology was determined by non-contact SFM. The results are shown in Fig. 4 for the CuPc/C<sub>60</sub> system deposited on SiO<sub>2</sub>/Si substrates and in Fig. 5 for the CuPc/F<sub>16</sub>CuPc material combination deposited on PEDOT:PSS/ITO/glass substrates. Neat films evaporated at room temperature display a granular structure which consists of crystallites of the respective material (see the X-ray scattering measurements below). The slight differences observed in neat CuPc films for the two different series in Figs. 4 and 5 are related to the interaction of the molecules with different substrates. Phthalocyanine films deposited at high temperatures have in both cases, a worm-like structure. The high temperature

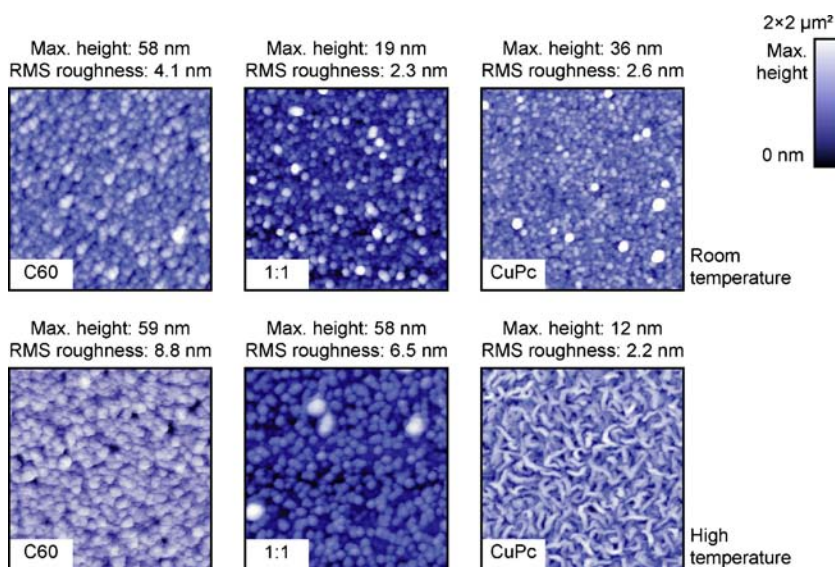


**Figure 4** (online color at: [www.pss-a.com](http://www.pss-a.com)) SFM images taken in non-contact mode for neat C<sub>60</sub> and CuPc films as well as for 1:1 blends grown at 300 K (upper row) and 375 K (lower row) deposited on SiO<sub>2</sub>/Si substrates. The total image size is 2 × 2  $\mu\text{m}^2$ . The maximum height is given as the difference between the lowest value (dark blue) and the highest value (white) in each of the images.

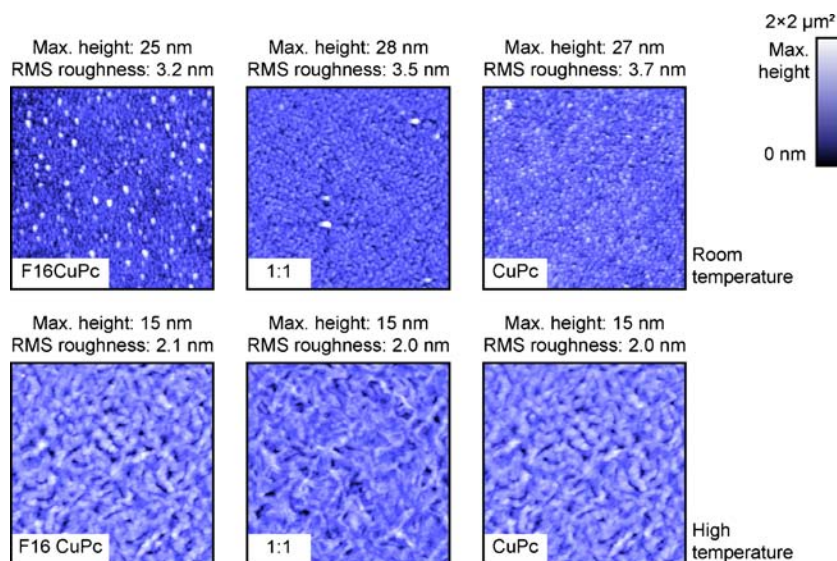


**Figure 5** (online color at: [www.pss-a.com](http://www.pss-a.com)) SFM images taken in non-contact mode for neat  $F_{16}CuPc$  and  $CuPc$  films as well as for 1:1 blends grown at 300 K (upper row) and 375 K (lower row) deposited on PEDOT:PSS. The total image size is  $2 \times 2 \mu m^2$ . The maximum height is given as the difference between the lowest value (dark blue) and the highest value (white) in each of the images.

during evaporation allows a faster diffusion of the molecules and thereby a better ordering resulting in these worm-like crystallites and a smoother film surface.

The roughness of the  $C_{60}$  films is in general higher than the one of the phthalocyanine films and increases further with higher substrate temperature during deposition. The same trend is observed for blended  $CuPc/C_{60}$  films where the measured height scale of about 58 nm for the heated blend exceeds the nominal film thickness of only about 25 nm. This observation can be related to demixing and phase separation between  $C_{60}$  and  $CuPc$  at elevated deposition temperature [26]. In contrast, the blended phthalocyanine films show the same morphology as the neat films and the roughness decreases for deposition at higher temperatures. We also analyzed the morphologies of two layer structures (not shown here). Thereby  $CuPc$  was evaporated first on PEDOT:PSS and then the acceptor on top of it. Whereas  $C_{60}$  forms rough films on top of  $CuPc$ , the  $F_{16}CuPc$  films have a similar morphology as on PEDOT:PSS, if a heated substrate is used. Thus, the different film morphologies of the two blend systems give the first hint toward different film growth modes, which will be discussed in more detail, further in the text.

Thin films of  $CuPc$  usually are present in the  $CuPc$   $\alpha$ -phase, determined earlier to be isostructural with other phthalocyanine  $\alpha$ -phases, which show a herringbone structure with two molecules per unit cell [27]. However, a later redetermination has shown that the  $CuPc$   $\alpha$ -phase has a triclinic structure with only one molecule per unit cell [28]. The  $CuPc$  molecules are standing nearly upright in evaporated films and stack in the direction parallel to the substrate. For growth on  $SiO_2$ ,  $F_{16}CuPc$  thin films exhibit two polymorphs coined  $\beta$ -phase and  $\beta_{bilayer}$ -phase [29, 30]. The two polymorphs exhibit different in-plane-stacking behavior, in particular the  $\beta$ -phase has a herringbone arrangement, where the  $\beta_{bilayer}$ -phase has a single molecule per unit cell and builds stacks parallel to the substrate similar to the  $CuPc$   $\alpha$ -phase. Since both  $F_{16}CuPc$  polymorphs have

an identical out-of-plane spacing, it cannot be determined by out-of-plane scattering, whether a herringbone arrangement is present in the neat film or not. Due to the different sizes of the terminating atoms, the size of the molecule varies and thereby also the lattice spacing  $a$ , perpendicular to the substrate (see Fig. 8) [28, 30]. The values are about 1.24 nm for the  $\alpha$ -phase of  $CuPc$  and about 1.43 nm for  $F_{16}CuPc$  films, respectively. Several other molecular arrangements have been observed, e.g.,  $CuPc$  crystallizes in a  $\beta$ -phase when heated higher than 480 K [31]. For the present study, the key point is not the subtle difference between different polymorphs, but rather the fact that the ordering motifs for both compounds are similar, thus facilitating the formation of mixed crystalline films.

$C_{60}$  thin films crystallize at room temperature in a face-centered cubic (fcc) lattice structure with a lattice constant of 1.417 nm [32, 33]. Thereby the (111) plane is mostly parallel to the substrate. Thermally evaporated  $C_{60}$  films usually contain only small grains with a small volume for coherent scattering; to increase the grain size deposition by hot wall, epitaxy is required [34].

To analyze the molecular arrangement in the films, X-ray scattering measurements were performed in  $\theta$ - $2\theta$  geometry. The obtained spectra are shown in Fig. 6. The diffraction peaks of both types of phthalocyanines are well pronounced. In contrast to previous measurements [16, 35], also the  $C_{60}$  diffraction peak is detectable due to the parallelized and monochromated incident beam.

The diffraction peaks of the  $CuPc/C_{60}$  blend have the same positions as the diffraction peaks of the respective neat films. These are related to the  $\alpha$ -phase of  $CuPc$  and the fcc structure of  $C_{60}$ . From this fact, we conclude that the blended film consists of both  $CuPc$  and  $C_{60}$  crystallites. This observation is in agreement with the SFM images discussed above and indicates the formation of a phase separated blend, which is related to the different molecular shape of the flat  $CuPc$  and the spherical  $C_{60}$ . The dimensions of the coexisting

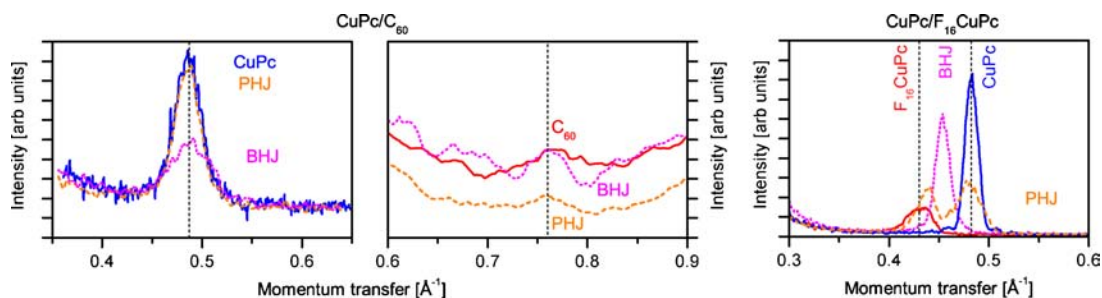


**Figure 6** (online color at: [www.pss-a.com](http://www.pss-a.com)) X-ray diffraction spectra for the CuPc/C<sub>60</sub> and the CuPc/F<sub>16</sub>CuPc material systems. The measurements for the neat films, the BHJ (mixing ratio 1:1) and the PHJ are shown. The films were evaporated on a PEDOT:PSS layer at room temperature. The different ranges of the momentum transfer for the CuPc/C<sub>60</sub> material combination were recorded with different statistics.

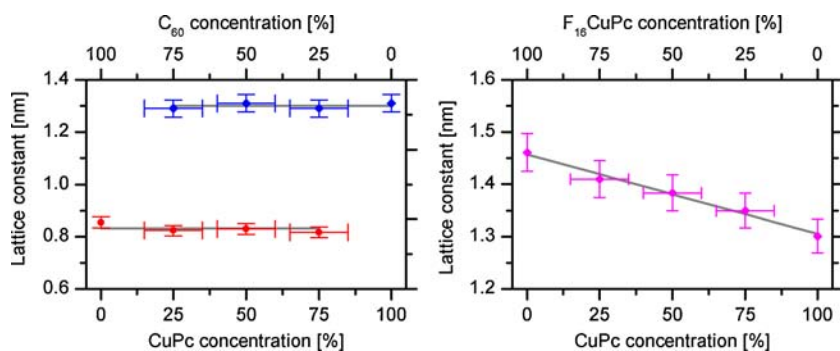


**Figure 7** (online color at: [www.pss-a.com](http://www.pss-a.com)) Analysis of the lattice spacing determined from Fig. 6 with dependence on the mixing ratio for the CuPc/C<sub>60</sub> blends (left) and the CuPc/F<sub>16</sub>CuPc blends (right). The gray lines are the average values (left) and the linear fit (right) of the measurement points.

crystallites are in the nanometer range (about 10 nm), consistent with the low peak intensities in the blends. The size of the phase separated crystallites can be varied by the substrate temperature during deposition or by the temperature of post-deposition annealing processes [36]. This is useful to optimize the internal interface for exciton dissociation in BHJ solar cells.

In contrast, the blended CuPc/F<sub>16</sub>CuPc film shows only one diffraction peak located between the diffraction peaks of the neat materials. Due to comparable crystal structures of both phthalocyanines, they are able to form a mixed crystalline film. Thereby the peak width is comparable to the neat films and the lattice spacing lies between the peaks of the neat materials. The dependence of the lattice parameter on the concentration is summarized in Fig. 7 for both DA systems. Additional blend ratios are included (3:1 and 1:3) which were not presented in Fig. 6 for clarity reasons. The system CuPc/C<sub>60</sub> shows for all blend ratios, the same lattice constants, being a clear indication of phase separation. The lattice constant for CuPc/F<sub>16</sub>CuPc changes linearly with the concentration between the lattice constants of the neat materials, consistent with a mixed crystalline film.

The spectra taken by X-ray scattering of the bilayered systems are also included in Fig. 6. Both acceptors, C<sub>60</sub> and F<sub>16</sub>CuPc, can be grown as crystalline films on top of the crystalline donor CuPc. The crystallinity of the phthalocyanines can be increased by evaporation of the films on a hot substrate (not shown). Thereby the increased crystallinity of CuPc acts as a template and leads to increased crystallinity of F<sub>16</sub>CuPc deposited on top.

Figure 8 shows schematic structures of films of neat phthalocyanines and a blended film. A gradual change of the lattice parameter in blends is related to the mixing of two molecular species with different size and a change of the tilt angle. Nevertheless, the observation of a single diffraction peak does not automatically imply the formation of an ordered mixed crystalline film with an in-plane superstructure (as one would guess from the figure). It merely indicates that both constituents are homogeneously mixed on a molecular scale.

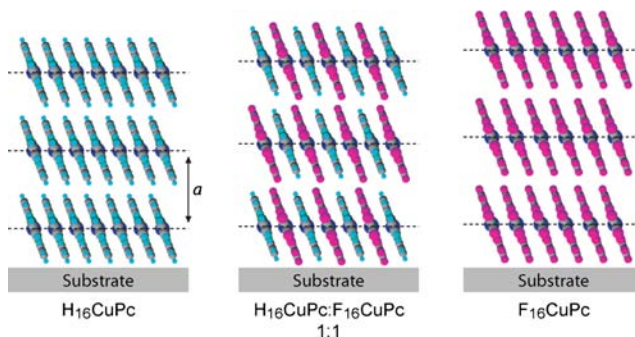


**Figure 8** (online color at: [www.pss-a.com](http://www.pss-a.com)) Schematic molecular arrangements for the neat and a mixed phthalocyanine film. The interlayer distance changes gradually from CuPc to the blend and further to F<sub>16</sub>CuPc. To visualize the structure of the blend, an ordered structure is assumed to be parallel to the substrate. The lattice parameter  $a$  is about 1.24 nm for the  $\alpha$ -phase in CuPc and about 1.4 nm for F<sub>16</sub>CuPc [28, 30].

Mixed crystals of evaporated molecules have also been observed for rod-like molecules [37]. The similar conjugated cores of sexithiophene, sexiphenyl, and dihexylsexithiophene together with the flexibility of the hexyl side chains allows for a gradual change of the lattice parameter with concentration. The conjugated system has a similar size also for the phthalocyanines used here. In contrast, the flat CuPc and the spherical C<sub>60</sub> with completely different  $\pi$ -conjugated systems form phase-separated blends. Another material system, showing phase separation, is the combination of rod-like pentacene and spherical fullerene [38]. However, different from the phthalocyanine/fullerene blends, which demix on a short scale (about 10 nm crystal size), the pentacene/fullerene blends are demixing on the length scale of the film thickness and can thus, not be used for photovoltaic applications.

**3.2 Optical properties** A prerequisite for efficient solar cells is absorption of light in a broad spectral range. We have thus analyzed the optical absorption for the two material systems in the UV–Vis range. Complementary and nearly non-overlapping absorption spectra are present for CuPc and C<sub>60</sub> in neat films as visible in Fig. 9 (left) [39]. This means that the absorption of the acceptor is high in a wavelength range where the absorption of the donor is low and vice versa. The absorption spectrum of the blend with a mixing ratio of 1:1 is also shown. It can be described quite well by an effective medium approximation [40]. The gray line gives an approximation for a blend with a concentration of 65% CuPc. This difference to the nominal ratio of 1:1 is related on the one hand to possible errors in the thickness determination of the neat films or to an error in the mixing ratio from the deposition process. Nevertheless, the phase separated CuPc/C<sub>60</sub> blend can be described as a mixture of crystallites composed of the neat materials and the intensity of all the peaks follows the concentration of the respective absorbing material. This fits very well into the framework of phase separation in CuPc/C<sub>60</sub> blends.

Overlapping absorption ranges are observed for the phthalocyanines (Fig. 9, right). As mentioned before, F<sub>16</sub>CuPc films crystallize in two different crystal structures [29, 30] with different absorption behavior. In the visible range, one structure is related to the peaks at 650 and 700 nm and the other structure has a large crystal shift resulting in a

peak around 795 nm [41]. The measured spectrum of the blend shows one strong peak at 620 nm and a shoulder at about 680 nm. These features are located in the spectral range where both molecules show absorption. In addition, the far red-shifted peak at 795 nm in F<sub>16</sub>CuPc disappears, indicating that the related packing motif is no longer present in the blend. Also the simulation using an effective medium approximation cannot describe the features of the blended film. This is another demonstration of the formation of mixed crystalline films by co-evaporation of the two different phthalocyanines and approves the structure model of the blend shown in Fig. 8.

**3.3 Electrical properties** Besides structural and optical properties, the charge carrier transport was also analyzed in these blend systems. Figure 10 shows current–voltage characteristics for hole-only, ambipolar, and electron-only devices of 1:1 blends of CuPc/C<sub>60</sub> and CuPc/F<sub>16</sub>CuPc as well as ambipolar characteristics for neat films, blends, and PHJs of both material combinations. Thereby the transport behavior is controlled by the choice of electrodes (see Table 1). The unipolar curves of the blends (part a and c) show almost no built-in voltage, while the ambipolar characteristics start at low voltages with a leakage current before the injected current dominates the  $I$ – $V$  curve of the CuPc/C<sub>60</sub> (CuPc/F<sub>16</sub>CuPc) blends at voltages higher than 0.4 V (0.25 V). This built-in voltage is related to the difference of the electrode work functions. The ambipolar current of the CuPc/C<sub>60</sub> blend is comparable to that of the electron transport in neat C<sub>60</sub>, which is much higher than the hole current in CuPc. For neat CuPc and C<sub>60</sub> films, the ambipolar  $I$ – $V$  curves show a built-in voltage which is higher than the built-in voltage of the 1:1 blend. The reduced built-in voltage of the blend might be related to the energy alignment at the organic/organic interface between CuPc and C<sub>60</sub> (see also Fig. 14).

Parts b and d compare the ambipolar currents of the neat materials with the respective BHJs and the PHJ for each material combination. Thereby a different behavior of the current in the blends is noticeable. The ambipolar current of the CuPc/C<sub>60</sub> blend is as high as the electron current in neat C<sub>60</sub>. In contrast, the ambipolar current in the blend of CuPc/F<sub>16</sub>CuPc is orders of magnitudes smaller than the ambipolar currents in the neat materials. These different characteristics will be discussed further below.

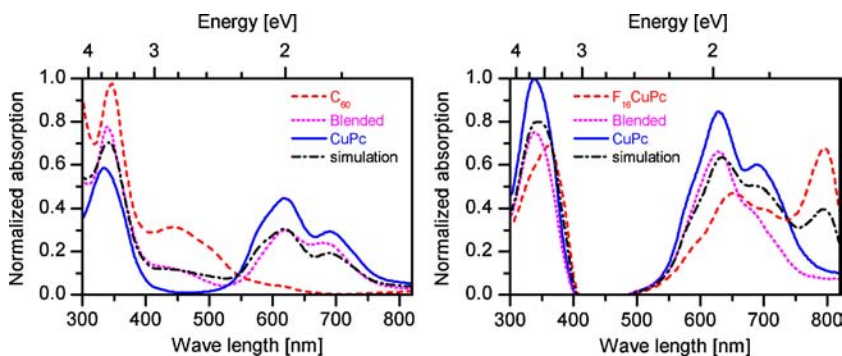


**Figure 9** (online color at: [www.pss-a.com](http://www.pss-a.com)) Optical absorption measurements of neat and 1:1 blended films with the CuPc/C<sub>60</sub> (left) and the CuPc/F<sub>16</sub>CuPc (right) material combinations in UV–Vis range as well as a simulation for the blend using an effective medium approximation.

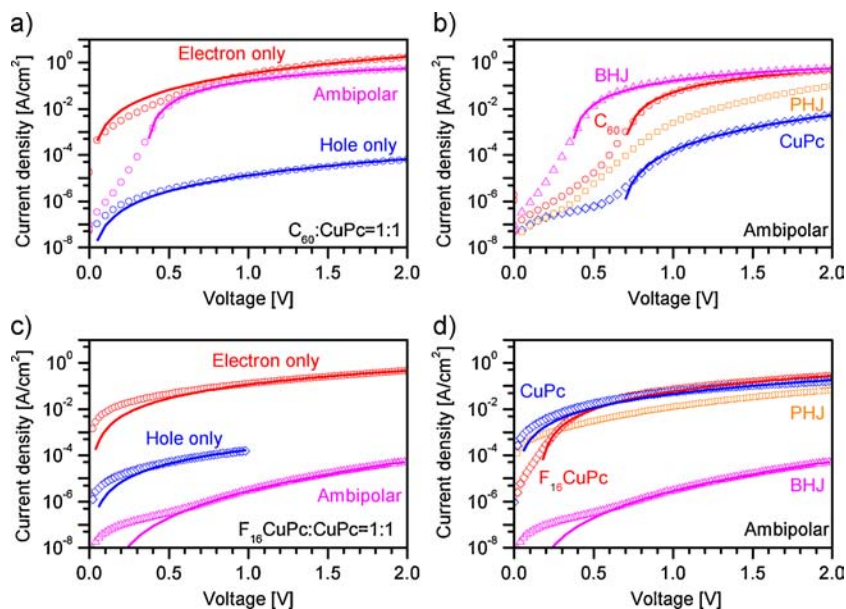


**Figure 10** (online color at: [www.pss-a.com](http://www.pss-a.com)) Current–voltage characteristics of different diode structures. The diagrams (a) and (c) compare unipolar and ambipolar transport of 1:1 blends of both material combinations. Ambipolar transport is shown for CuPc/C<sub>60</sub> (b) and CuPc/F<sub>16</sub>CuPc (d) blends and the respective neat films together with the PHJs. The solid lines are fits using an SCLC model as described in the text. The films for the CuPc/C<sub>60</sub> system were evaporated on substrates kept at room temperature, the other material combination was grown on the substrate at 375 K.

Additionally, we have also measured ambipolar  $I$ – $V$  characteristics of PHJs of both material combinations. Whereas the CuPc/C<sub>60</sub> two layer structure displays a typical diode behavior, the CuPc/F<sub>16</sub>CuPc system shows higher currents under backward than under forward biasing (for details see Ref. [42]). This can be related to the formation of a charge generation layer at the organic–organic interface as described in the literature for other material combinations where the donor has an ionization potential close to the electron affinity of the acceptor [43, 44].

Using the SCLC model with a field-dependent mobility (see Eq. (2)), the zero-field mobilities have been determined for the neat and blended films of the CuPc/C<sub>60</sub> (Fig. 11a) and the CuPc/F<sub>16</sub>CuPc (Fig. 11b) material combinations. The field-activation parameter  $\gamma$  is very low (or even zero) in both cases and therefore negligible [12]. The resulting mobilities for CuPc/C<sub>60</sub> decrease exponentially by dilution of the respective transport material with the other species [12]. With the used electrode materials, the transport of both charge carrier types is observed in C<sub>60</sub> as well as CuPc. However, the unipolar mobilities depend strongly on the

mixing ratio. The electron mobility decreases exponentially with decreasing C<sub>60</sub> content and in the neat CuPc film a further reduction of the mobility occurs. From this it can be deduced, that the electron transport in the blends is carried by the C<sub>60</sub> molecules only. By mixing, the hopping distances are increased and as a result the mobilities decrease exponentially. In this case the mobility limiting step would be the hopping between grains where the average distance between the phase separated crystallites should also increase upon dilution. This is well-established for molecularly doped polymers [45], where a homogenous dilution of conducting molecules in an inert matrix is present. This scenario might even hold for nano-phase separated granular films. The strong mobility decrease between the mixed film with the lowest C<sub>60</sub> content and the neat CuPc film is related to the much lower electron mobility in neat CuPc. In contrast, the hole mobility changes over the whole concentration range uniformly, as the difference in the hole mobility between the two materials is much smaller. As aforementioned, both molecular materials can transport electrons as well as holes in the used electrode configuration. Using an

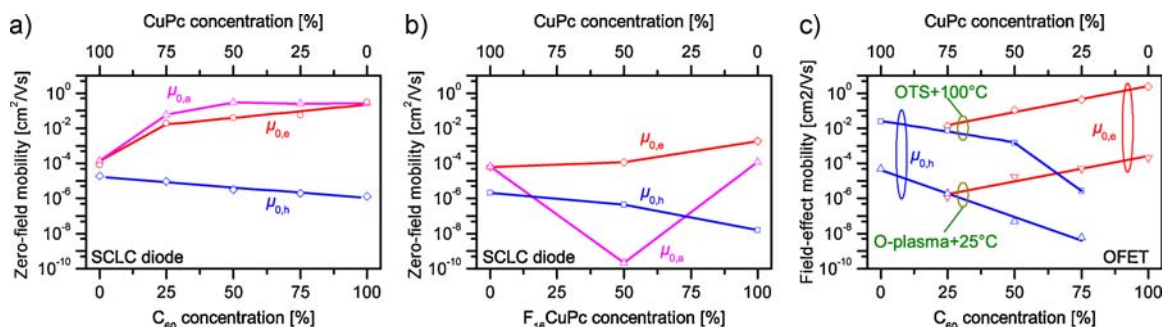


**Figure 11** (online color at: [www.pss-a.com](http://www.pss-a.com)) Zero-field mobilities determined from the SCLC model including a field-dependent mobility for neat and blended films of CuPc/C<sub>60</sub> (a) and CuPc/F<sub>16</sub>CuPc (b). Field-effect mobilities (c) determined from saturation regime as function of concentration, substrate temperature and treatment for blend of C<sub>60</sub>/CuPc.

electron and a hole injecting electrode, ambipolar transport occurs. The determined mobility for this ambipolar transport (shown also in Fig. 11) is higher than the sum of the unipolar hole and electron mobilities. This should be related to the ambipolar nature of both materials [20]. Nevertheless the transport in the blended films is based mainly on the transport of electrons by the  $C_{60}$  molecules. Conductive paths of the spherical  $C_{60}$  molecules are also expected in the presence of the planar stacked CuPc molecules in the mixture [11].

The unipolar mobilities of the blended CuPc/ $F_{16}$ CuPc film are located between the unipolar mobilities of the neat films as shown in Fig. 11b. The gradual change of the concentration in this mixed system results also in a gradual change of the unipolar mobilities. However, the ambipolar mobility in the blended film is orders of magnitude lower than both unipolar mobilities and the ambipolar mobilities of the neat materials. As the unipolar mobilities are high, the ambipolar transport cannot be limited by the absence of percolation paths. Therefore, the strongly reduced ambipolar mobility should be related to the presence of both charge carrier types at the same time. A tentative explanation is the generation of charge transfer excitons by the injected charge carrier pairs. These charge transfer excitons will limit the transport by blocking the occupied molecules for further injected charge carriers (for details see Ref. [42]). The different transport behavior is summarized in Fig. 12.

The charge carrier mobilities of CuPc/ $C_{60}$  were also measured in OFETs [16, 25]. Due to the sign of the applied effective gate voltage, the accumulation of electrons and holes can be chosen separately. The unipolar mobilities of this blend are shown in Fig. 11 (diagram at the right). No ambipolar transport was observed in the OFET geometry for the neat molecular films. The field-effect mobilities in blends also decrease exponentially with decreasing concentration of the respective transport material. Remarkably, all blends with different mixing ratios show charge carrier transport for

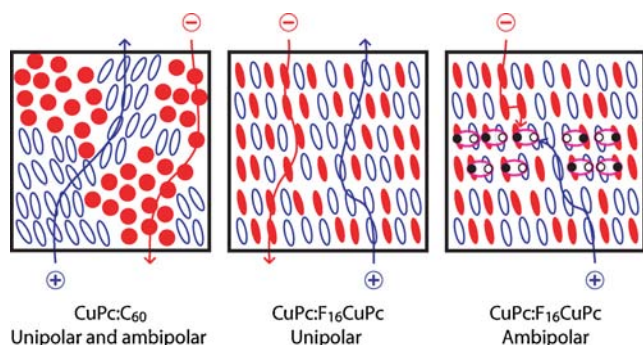


**Figure 12** (online color at: [www.pss-a.com](http://www.pss-a.com)) Schematics for the unipolar and ambipolar transport through blends of CuPc/ $C_{60}$  (left), unipolar transport through blends of CuPc/ $F_{16}$ CuPc (middle), and ambipolar transport through blends of CuPc/ $F_{16}$ CuPc (right). The transport in CuPc/ $C_{60}$  blends occurs via percolation pathways between grains of the separated materials in both the unipolar and ambipolar case. The ambipolar transport in molecularly mixed CuPc/ $F_{16}$ CuPc blends is limited by the formation of charge transfer excitons, which are absent if only one charge carrier type is injected.

both charge carrier types. This means that there is always a percolation path for both electrons and holes. However, the hopping distance between molecules of the same type is increased upon mixing with the other species as reported above for diodes. As compared to film growth at room temperature, an increased mobility is found for the higher substrate temperature (not shown, Ref. [25]) and a further increase is realized by lowering the surface energy with octadecyltrichlorosilane (OTS) together with high temperature deposition. This increase in mobility was reported for unipolar OFETs [46] and is also valid for these blends. Interestingly, for all treatment balanced mobilities are found at about 25%  $C_{60}$  content which is important for an application of these ambipolar OFETs in ambipolar inverters [16, 25].

The mobilities of the CuPc/ $C_{60}$  blends in OFETs change more drastically, by dilution, than in diodes. From the exponential reduction with decreasing concentration of the respective transport material, percolation between the grains is identified as the limiting factor for charge transport in these blends. The comparison of transport in a diode with transport in an OFET supports this. In the latter, transport occurs at the interface between the insulator and the semiconductor inside the accumulation layer and is thus limited to a 2D area. On the other hand, transport in diodes is 3D, because there is no limitation of the charge carrier distribution in the third dimension between the two electrodes. Transferred to the transport in molecular blends, a higher number of neighboring molecules results in a larger number of transport pathways in the 3D system. Therefore transport in diodes is less reduced by mixing, in contrast to the transport in OFETs.

**4 Photovoltaic cells** Organic donor and acceptor materials are promising candidates for photovoltaic cells. In these cells the generated excitons dissociate into free charge carriers at the DA interface by an ultra-fast photo-induced charge transfer [5]. To create this active interface PHJ [7] and BHJ [8, 47], photovoltaic cells have been employed. These two different architectures are shown in Fig. 13. In PHJ cells, the dissociation interface is localized between the two layers, while the dissociation in the BHJ cells occurs within the whole volume of the blended film. Due to this mixture of donor and acceptor materials, the

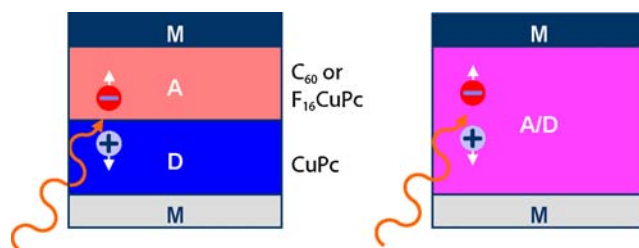


**Figure 13** (online color at: [www.pss-a.com](http://www.pss-a.com)) Side view of the PHJ (left) and BHJ (right) solar cell, including metal electrodes (M), the donor (D), and the acceptor (A) molecules. Additionally the charge transport is sketched.

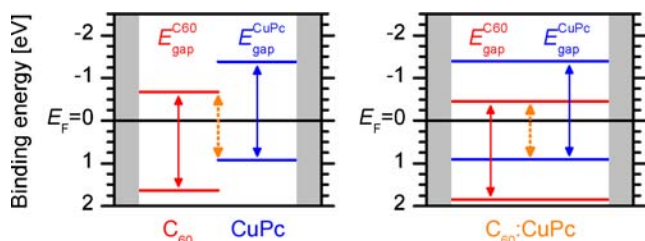


**Figure 14** (online color at: [www.pss-a.com](http://www.pss-a.com)) Schematic energy diagram for the PHJ (left side) and BHJ (right side) of the material system CuPc/C<sub>60</sub>. The transport gap is 2.3 eV for both neat materials [48, 49], which is also assumed for the mixture [50, 12]. The Fermi energy is related to the conductive substrate PEDOT:PSS. The dashed arrow indicates the magnitude of the intermolecular HOMO–LUMO gap of 1.6 eV for the PHJ and 1.35 eV for the BHJ.

photon-to-current conversion efficiency and the power conversion efficiency are expected to increase [8, 47, 39].

In the following discussion, PHJ and BHJ devices will be compared. Of particular interest will be the difference in the open circuit voltage between the two types of solar cells. As reported previously [48, 12], the intermolecular gap between the HOMO of the donor and the LUMO of the acceptor, which is an important parameter for the open circuit voltage of a solar cell, is reduced in blends of CuPc/C<sub>60</sub> in comparison to the bilayered system. This change is related to the gradual shift of the common vacuum level with the composition of the blend [48]. Together with a constant ionization potential, an unchanged transport gap (for both molecules it is 2.3 eV [49, 50]) leads to the reduced intermolecular gap as shown in Fig. 14. The obtained values for the intermolecular gap are 1.6 and 1.35 eV for the two-layer and the blended system, respectively. However, it is noteworthy that the energy levels displayed in this figure do not describe the real interface behavior. While there is no band bending at the organic/organic interface [51], which is the relevant one for photovoltaic cells, the electrode/organic interfaces are shown only schematically in Fig. 14 without interface dipoles or possible band bending.

The current–voltage characteristics of both types of CuPc/C<sub>60</sub> cells are shown in Fig. 15a,b for different light

intensities. The crossing point of the curves for all the different light intensities is the compensation voltage  $V_{Comp}$  [52] where the dark current and the photocurrents are equal. This compensation voltage is about 0.55 eV for the PHJ cell and about 0.35 eV for the BHJ device. The difference of the compensation voltages for the two systems is only a little smaller than the difference between the intermolecular HOMO–LUMO gaps determined by ultraviolet photoelectron spectroscopy (UPS) measurements. The open circuit voltages ( $V_{OC}$ ) for the different light intensities are collected in Fig. 16 on the left side. Over the whole range of light intensities, the open circuit voltage in the bilayered cell is about 0.2 V higher than in the blended system. This effect was already observed in the CuPc/C<sub>60</sub> system at high illumination intensities [11], as well as for other material combinations using small molecules [53] or polymers [54]. The open circuit voltage is therefore related to the gap between the LUMO of the acceptor and the HOMO of the donor [55]. Both the measured open circuit voltage and the compensation voltage are smaller for the blended system as expected from the UPS measurements. However, the open circuit voltage is significantly smaller than the intermolecular gap. This is related to further losses inside the organic photovoltaic cell [55]. Nevertheless, changes of the electronic levels of the donor and acceptor molecules are seen directly as a change of the open circuit voltage.

Figure 16 also compares the short circuit current density ( $J_{SC}$ ) of both cell types of the CuPc/C<sub>60</sub> material combination. The BHJ solar cell is providing the higher short circuit current. The reason is that by mixing of the molecules, a distributed donor/acceptor interface is formed within the organic film. Thereby it is possible for nearly all excitons to reach the DA interface to dissociate even for a short exciton diffusion length [9, 10]. It is remarkable that the short circuit currents for the BHJ cells are higher than for the PHJ devices, even though the mobility in the blended system is by far lower than in the neat films as described above and in the literature [11, 16]. The fill factor reaches 32% for the bilayered and the blended cell at a light intensity of about 100 mW/cm<sup>2</sup>. Due to series resistances and recombination losses, the power conversion efficiency is rather low in our

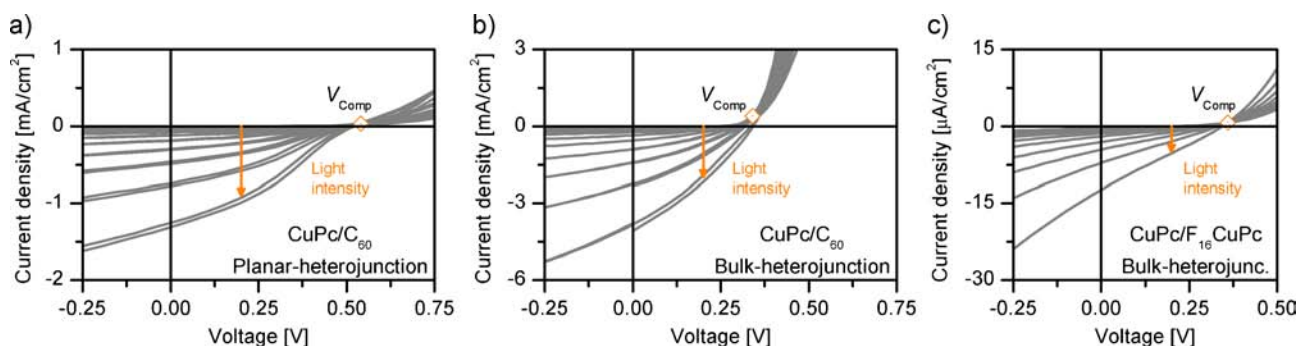


**Figure 15** (online color at: [www.pss-a.com](http://www.pss-a.com)) Current–voltage characteristics for the analyzed solar cells. From left to right: PHJ cell of CuPc/C<sub>60</sub>, BHJ cell of CuPc/C<sub>60</sub>, BHJ cell of CuPc/F<sub>16</sub>CuPc. The curves are shown for different light intensities up to one sun. The compensation voltage  $V_{Comp}$  is determined as the crossing point of all curves for different light intensities [51].

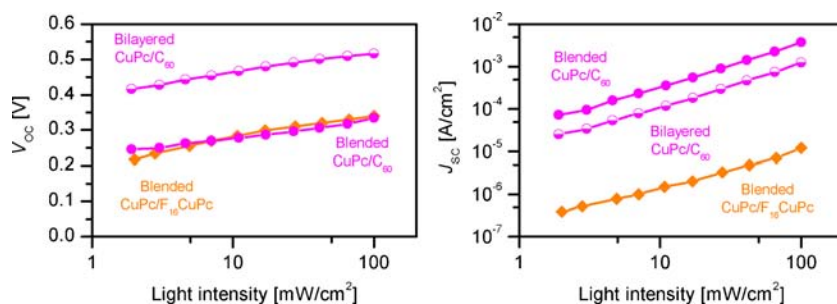


**Figure 16** (online color at: www.pss-a.com) Open circuit voltage ( $V_{OC}$ ) and short circuit current density ( $J_{SC}$ ) for PHJ and BHJ solar cells using CuPc/ $C_{60}$  and for a BHJ solar cell using CuPc/ $F_{16}$ CuPc as function of the white light intensity (AM1.5 standard). The symbols are determined from the measurements shown in Fig. 15. The lines are to guide the eyes.

cells (at the highest intensity 0.4% for the blended and maximal 0.2% for the PHJ solar cell).

Figure 15c shows the  $I$ - $V$  characteristics for a solar cell containing a blended CuPc/ $F_{16}$ CuPc film as active layer. The measurements include the dark current and the current under various illumination intensities. The analysis of the open circuit voltage and the short circuit current is included in Fig. 16. The compensation voltage is about 0.35 eV and is comparable to the compensation voltage of the blended CuPc/ $C_{60}$  cell. The current densities, however, are about two orders of magnitude lower in the blended CuPc/ $F_{16}$ CuPc cell in comparison to the CuPc/ $C_{60}$  BHJ solar cell. Regarding the low ambipolar mobility in the CuPc/ $F_{16}$ CuPc blends, the very low photocurrents could also be related to a self-trapping process of photo-generated charge transfer excitons instead of injected ones. A fill factor of about 25% and a power conversion efficiency of only 0.002% shows the low performance and limited usability of this system in photovoltaic cells. Furthermore, the bilayered system CuPc/ $F_{16}$ CuPc (not shown here) does not have an effect of illumination at all [42].

**5 Summary** The analyzed blends of hole and electron conducting materials show different layer formation behavior. The system CuPc/ $C_{60}$  forms separated phases of each material with percolation pathways for the transport of opposite charge carriers through the blend. Thereby the hopping distance between crystalline grains limits the transport. As a consequence, the mobilities decrease exponentially in both diodes and OFETs, upon diluting the respective transport material with the other species. In this system the obtained electron mobility is much higher than the hole mobility in the neat materials as well as in the blends. For this reason, the current in blended films is mainly based on the electron transport through  $C_{60}$  clusters. In contrast, blends of the two phthalocyanines CuPc and  $F_{16}$ CuPc, form molecularly mixed crystalline films with a gradual change of the lattice parameter by changing the mixing ratio. Also the unipolar mobilities of both charge carrier types show a gradual change between the mobilities of the neat materials. The ambipolar mobility of the blends, however, is reduced drastically. This could be related to the generation of charge transfer excitons in neighboring CuPc and  $F_{16}$ CuPc molecules. These CT excitons can only be created if both charge carrier types are injected at the same time.

Both material combinations have also been analyzed in PHJ and BHJ solar cells. While PHJ solar cells are limited by the exciton diffusion efficiency  $\eta_{ED}$  due to the low active volume, this restriction is absent for BHJ cells. However, in the latter, charge transport is limited by the size of grains which are necessary to form percolation pathways in phase separated blends. Thus, for a further increase in the efficiency of CuPc/ $C_{60}$  BHJ solar cells, the DA interface needs to be optimized in order to allow for both a high exciton diffusion efficiency  $\eta_{ED}$  and a reasonable charge collection efficiency  $\eta_{CC}$  via charge transport of both charge carriers. In contrast, in BHJ devices of CuPc/ $F_{16}$ CuPc, the major obstacle is seen in a very low exciton dissociation efficiency  $\eta_{CT}$  which is reduced by the formation of charge transfer excitons. Thus the material combination of hydrogenated and fluorinated phthalocyanines is not suitable for the application in photovoltaic cells.

**Acknowledgements** This work was supported by the Deutsche Forschungsgemeinschaft through priority program 1355. The authors thank Jens Pflaum (Universities of Stuttgart and Würzburg) for purifying organic materials. Stefan Krischok, Marcel Himmerlich, Pierre Lorenz, and Juergen A. Schaefer (Technical University of Ilmenau) have supported the photoelectron spectroscopy measurements. We acknowledge contributions by Marcel Götzenbrunner, Bernhard Ecker, and Markus Bronner for experimental characterization.

## References

- [1] M. Schwoerer, and H. C. Wolf, *Organic Molecular Crystals* (Wiley-VCH, Weinheim, 2007).
- [2] W. Brütting, (ed.), *Physics of Organic Semiconductors* (Wiley-VCH, Weinheim, 2005).
- [3] D. Jérôme, and H. Schulz, *Adv. Phys.* **31**, 299–490 (1982).
- [4] Y. Takahashi, T. Hasegawa, Y. Abe, Y. Tokura, and G. Saito, *Appl. Phys. Lett.* **88**, 073504 (2006).
- [5] N. S. Sariciftci, L. Smilowitz, A. J. Heeger, and F. Wudl, *Science* **258**, 1474–1476 (1992).
- [6] S. Forrest, *MRS Bull.* **30**, 28–32 (2005).
- [7] C. W. Tang, *Appl. Phys. Lett.* **48**, 183–185 (1986).
- [8] J. Rostalski, and D. Meissner, *Sol. Energy Mater. Sol. Cells* **61**, 87–95 (2000).
- [9] B. P. Rand, J. Genoe, P. Heremans, and J. Poortmans, *Prog. Photovolt.: Res. Appl.* **15**, 659–676 (2007).
- [10] P. Peumans, A. Yakimov, and S. R. Forrest, *J. Appl. Phys.* **93**, 3693–3723 (2003).

- [11] J. G. Xue, B. P. Rand, S. Uchida, and S. R. Forrest, *J. Appl. Phys.* **98**, 124903 (2005).
- [12] A. Opitz, M. Bronner, J. Wagner, M. Götzenbrugger, and W. Brütting, *Proc. SPIE* **7002**, 70020J (2008).
- [13] I. Salzmann, R. Opitz, S. Rogaschewski, J. P. Rabe, N. Koch, and B. Nickel, *Phys. Rev. B* **75**, 174108 (2007).
- [14] A. K. Pandey, and J. M. Nunzi, *Appl. Phys. Lett.* **89**, 213506 (2006).
- [15] R. Schueppel, K. Schmidt, C. Uhrich, K. Schulze, D. Wynands, J. L. Brédas, E. Brier, E. Reinold, H. B. Bu, P. Baeuerle, B. Maennig, M. Pfeiffer, and K. Leo, *Phys. Rev. B* **77**, 085311 (2008).
- [16] A. Opitz, M. Bronner, and W. Brütting, *J. Appl. Phys.* **101**, 063709 (2007).
- [17] M. A. Loi, C. Rost-Bietsch, M. Murgia, S. Karg, W. Rieß, and M. Muccini, *Adv. Func. Mater.* **16**, 41–47 (2006).
- [18] L. L. Chua, J. Zaumseil, J. F. Chang, E. C. W. Ou, P. K. H. Ho, H. Sirringhaus, and R. H. Friend, *Nature* **434**, 194–199 (2005).
- [19] E. C. P. Smits, T. D. Anthopoulos, S. Setayesh, E. van Veenendaal, R. Coehoorn, P. W. M. Blom, B. de Boer, and D. M. de Leeuw, *Phys. Rev. B* **73**, 205316 (2006).
- [20] A. Opitz, M. Kraus, M. Bronner, J. Wagner, and W. Brütting, *New J. Phys.* **10**, 065006 (2008).
- [21] W. Brütting, S. Berleb, and A. G. Muckl, *Org. Electron.* **2**, 1–36 (2001).
- [22] Y. Abe, T. Hasegawa, Y. Takahashi, T. Yamada, and Y. Tokura, *Appl. Phys. Lett.* **87**, 153506 (2005).
- [23] N. Mott, and R. Gurney, *Electronic Processes in Ionic Crystals* (Clarendon Press, Oxford, 1940).
- [24] P. Murgatroyd, *J. Phys. D: Appl. Phys.* **3**, 151–156 (1970).
- [25] M. Bronner, A. Opitz, and W. Brütting, *Phys. Status Solidi A* **205**, 549–563 (2008).
- [26] M. Stöhr, T. Wagner, M. Gabriel, B. Weyers, and R. Möller, *Adv. Func. Mater.* **11**, 175–178 (2001).
- [27] M. Ashida, N. Uyeda, and E. Suito, *J. Chem. Soc. Jpn.* **39**, 2616–2624 (1966).
- [28] A. Hoshino, Y. Takenaka, and H. Miyaji, *Acta Crystallogr. B* **59**, 393–403 (2003).
- [29] J. O. Ossó, F. Schreiber, V. Kruppa, H. Dosch, M. Garriga, M. I. Alonso, and F. Cerdeira, *Adv. Func. Mater.* **12**, 455–460 (2002).
- [30] D. G. de Oteyza, E. Barrena, J. O. Ossó, S. Sellner, and H. Dosch, *J. Am. Chem. Soc.* **128**, 15052–15053 (2006).
- [31] J. Y. E. , S. Kim, E. J. Lim, K. J. Lee, D. J. Cha, and B. Friedman, *Appl. Surf. Sci.* **205**, 274–279 (2003).
- [32] D. Faiman, S. Goren, E. A. Katz, M. Koltun, N. Melnik, A. Shames, and S. Shtutina, *Thin Solid Films* **295**, 283–286 (1997).
- [33] A. F. Hebard, R. C. Haddon, R. M. Fleming, and A. R. Kortan, *Appl. Phys. Lett.* **59**(17), 2109–2111 (1991).
- [34] D. Stifter, and H. Sitter, *Appl. Phys. Lett.* **66**, 679–681 (1995).
- [35] B. P. Rand, J. G. Xue, S. Uchida, and S. R. Forrest, *J. Appl. Phys.* **98**, 124902 (2005).
- [36] P. Peumans, S. Uchida, and S. Forrest, *Nature* **425**, 158–162 (2003).
- [37] J. O. Vogel, I. Salzmann, R. Opitz, S. Duhm, B. Nickel, J. P. Rabe, and N. Koch, *J. Phys. Chem. B* **111**, 14097–14101 (2007).
- [38] I. Salzmann, S. Duhm, R. Opitz, R. L. Johnson, J. P. Rabe, and N. Koch, *J. Appl. Phys.* **104**, 114518 (2008).
- [39] T. Stübinger, and W. Brütting, *Proc. SPIE* **4465**, 102–112 (2002).
- [40] D. Datta, V. Tripathi, P. Gogoi, S. Banerjee, and S. Kumar, *Thin Solid Films* **516**, 7237–7240 (2008).
- [41] M. I. Alonso, M. Garriga, J. O. Ossó, F. Schreiber, E. Barrena, and H. Dosch, *J. Chem. Phys.* **119**, 6335–6340 (2003).
- [42] A. Opitz, B. Ecker, J. Wagner, A. Hinderhofer, F. Schreiber, J. Manara, J. Pflaum, and W. Brütting, *Org. Electron.* **10**, 1259–1267 (2009).
- [43] M. Kröger, S. Hamwi, J. Meyer, T. Dobbertin, T. Riedl, W. Kowalsky, and H. H. Johannes, *Phys. Rev. B* **75**, 235321 (2007).
- [44] B. Yu, F. Zhu, H. Wang, G. Li, and D. Yan, *J. Appl. Phys.* **104**, 114503 (2008).
- [45] P. M. Borsenberger, and D. S. Weiss, *Organic Photoreceptors for Imaging Systems* (Marcel Dekker Ltd., New York, 1993).
- [46] C. K. Song, B. W. Koo, S. B. Lee, and D. H. Kim, *Jpn. J. Appl. Phys.* **41**, 2730–2734 (2002).
- [47] G. Yu, J. Gao, J. C. Hummelen, F. Wudl, and A. J. Heeger, *Science* **270**, 1789–1791 (1995).
- [48] A. Opitz, M. Bronner, W. Brütting, M. Himmerlich, J. A. Schaefer, and S. Krischok, *Appl. Phys. Lett.* **90**, 212112 (2007).
- [49] I. Hill, A. Kahn, Z. Soos, and R. Pascal, *Chem. Phys. Lett.* **327**, 181–188 (2000).
- [50] R. W. Lof, M. A. Vanveenendaal, B. Koopmans, H. T. Jonkman, and G. A. Sawatzky, *Phys. Rev. Lett.* **68**, 3924–3927 (1992).
- [51] O. V. Molodtsova, and M. Knupfer, *J. Appl. Phys.* **99**, 053704 (2006).
- [52] V. D. Mihailetchi, L. J. A. Koster, J. C. Hummelen, and P. W. M. Blom, *Phys. Rev. Lett.* **93**, 216601 (2004).
- [53] C. Melzer, V. V. Krasnikov, and G. Hadziioannou, *J. Polym. Sci. B* **41**, 2665–2673 (2003).
- [54] Y. Hayashi, I. Yamada, S. Takagi, A. Takasu, T. Soga, and T. Jimbo, *Jpn. J. Appl. Phys.* **44**, 1296–1300 (2005).
- [55] C. J. Brabec, V. Dyakonov, J. Parisi, and N. S. Sariciftci (eds.) *Organic Photovoltaics Semiconductor Aspects of Organic Bulk Heterojunction Solar Cells* (Springer, Berlin, 2003), pp. 159–248.